This is a repository copy of *Oxygen redox activity in battery cathodes and the role of underbonded oxygen*.

White Rose Research Online URL for this paper:
https://eprints.whiterose.ac.uk/219779/

Version: Published Version

Article:
West, A. orcid.org/0000-0002-5492-2102, Zhao, Y.R., Middlemiss, L.R. et al. (2 more authors) (2024) Oxygen redox activity in battery cathodes and the role of underbonded oxygen. Zeitschrift für anorganische und allgemeine Chemie, 650 (23). e202400067. ISSN 0044-2313

https://doi.org/10.1002/zaac.202400067

Reuse
This article is distributed under the terms of the Creative Commons Attribution (CC BY) licence. This licence allows you to distribute, remix, tweak, and build upon the work, even commercially, as long as you credit the authors for the original work. More information and the full terms of the licence here: https://creativecommons.org/licenses/

Takedown
If you consider content in White Rose Research Online to be in breach of UK law, please notify us by emailing eprints@whiterose.ac.uk including the URL of the record and the reason for the withdrawal request.

eprints@whiterose.ac.uk
https://eprints.whiterose.ac.uk/

Journal of Inorganic and General Chemistry
ZAAC
Zeitschrift für anorganische und allgemeine Chemie
www.zaac.wiley-vch.de
RESEARCH ARTICLE

Check for updates

DOI: 10.1002/zaac.202400067

Oxygen Redox Activity in Battery Cathodes and the Role of Underbonded Oxygen

Yangyang Zhao,[a] Laurence Middlemiss,[a] Xuan Zhi,[a] Peter Gross,[a] and Anthony R West[a]

Dedicated to Martin Jansen on the occasion of his 80th birthday.

It is widely recognised that oxygen redox makes a significant contribution to the high capacity of some cathode materials in addition to the more usual transition metal redox. We attribute this to the presence of underbonded oxide ions, either in bulk structures or at surfaces, which act as the initial source of oxygen redox during charging. Underbonded oxide ions experience departures from local electroneutrality; examples include $Li_4Mn_5O_{12}$ spinel and Li-rich layered rock salt structures but not stoichiometric $LiCoO_2$ or Li_2MnO_3. Underbonded oxide ions ionise more readily than fully-stabilised lattice oxide ions since, using an ionic bonding description, they are associated with a deficiency of positive charge in the coordination sphere of surrounding cations. Pauling's electrostatic bond strength criterion gives a simple guide to structures or compositions that may show departures from local electroneutrality and provides the starting point for a new way to consider oxygen redox. $Li_4Mn_5O_{12}$ behaves as an anode due to Mn redox below 3 V but also behaves as a cathode due to reversible oxygen redox above ~3.8 V. In the high symmetry cubic structure of $Li_4Mn_5O_{12}$, depending on the local distribution of cations over the occupied tetrahedral and octahedral sites, some oxygens are inevitably underbonded whereas others must be over-bonded, although none show local electroneutrality expected from the average crystal structure. Underbonded oxygens are also identified in other structures, including high capacity Li-rich layered rock salt structures.

Introduction

Since the first report of reversible oxygen redox in lithium ion battery cathode materials,[1] oxygen redox activity has been, with a few notable exceptions,[2] widely recognised as contributing to the performance of certain high capacity lithium and sodium battery cathodes.[3] It has not been possible to predict and rationalise which materials could show oxygen redox, in particular during the initial charge process. For example, within the large family of rock salt-related structures, $LiCoO_2$[4] does not show reversible oxygen redox under usual charge-discharge conditions, whereas some of the newer cathode materials, such as Li-rich layered rock salt oxides,[5] numerous nonstoichiometric layered rock salt Na oxides[6] and some disordered rock salt oxides,[7] do have both redox-active oxygen and the usual, redox-active transition metals.

Oxygen redox based on the O^{2-} ion may occur in two main stages.[8,12] The first stage involves loss of one electron leaving behind a hole that is either localised as a small polaron on one specific oxygen,[9,10] or delocalised over several[11] lattice oxygen atoms. The second stage involves loss of another electron; the association of two doubly ionised oxygen atoms then leads to the generation of molecular O_2.[12] In some cases, there is evidence that these molecules may be trapped in voids within the cathode lattice,[9,10] but usually it is irreversibly lost, either directly as O_2 gas,[8] or as singlet oxygen atoms that oxidise solvent molecules of the electrolyte.[13] While the two stages can occur at different potentials and therefore sequentially in some materials, like $Li_{1.20}Mn_{0.54}Co_{0.13}Ni_{0.13}O_2$,[14] resulting in the first stage of anionic redox occurring homogeneously over the bulk of the oxide sublattice and loss of the second electron and generation of O_2 attributed to reaction of surface oxide ions,[15] in many cases both oxygen redox stages occur simultaneously, for example when O_2 gas is evolved directly from O^{2-} ions in crystal lattices as a result of either reduction or equilibration with the atmosphere at high temperature.[12] In order to utilise oxygen redox in reversible batteries, it is essential that only the first stage occurs; as yet, this is often not achieved in isolation and consequently, material performances degrade due to oxygen loss on cycling.

There is much discussion in the literature concerning the mechanism(s) of oxygen redox. The nature of the intermediate species between O^{2-} and O_2 may simply be O^- ions, catenated species such as O_2^{2-} or more generally, O_2^{n-}. Evidence for the different species is usually circumstantial, especially in cathode materials that are in a state of partial charge or discharge, although modelling studies on the intrinsic delithiation mechanism in Li_2MnO_3 involves oxidation at the oxygen site leading to the formation of bound oxygen hole polarons,[17] i.e. localised O^- ions. We do not enter further into that discussion here and refer to the intermediate species generally as O^- ions.

In all the discussions and speculation about anion redox, one factor that appears to have been overlooked is whether the

[a] Y. Zhao, L. Middlemiss, X. Zhi, P. Gross, A. R West
Department of Materials Science & Engineering, University of Sheffield, Mappin Street, Sheffield S1 3JD, UK

© 2024 The Author(s). Zeitschrift für anorganische und allgemeine Chemie published by Wiley-VCH GmbH. This is an open access article under the terms of the Creative Commons Attribution License, which permits use, distribution and reproduction in any medium, provided the original work is properly cited.

 © 2024 The Author(s). Zeitschrift für anorganische und allgemeine Chemie published by Wiley-VCH GmbH

15213749, 0, Downloaded from https://onlinelibrary.wiley.com/doi/10.1002/zaac.202400067 by UNIVERSITY OF SHEFFIELD, Wiley Online Library on [19/11/2024]. See the Terms and Conditions (https://onlinelibrary.wiley.com/terms-and-conditions) on Wiley Online Library for rules of use; OA articles are governed by the applicable Creative Commons License

cationic environment around oxygen meets the (ideal) requirements for local electroneutrality - somewhat surprisingly, given that bond-length/bond-strength arguments were employed to explain ionic diffusion in the very same materials.[18] Certainly, the nature of the cation environment around oxygen features in discussions on possible oxygen redox and the location of holes.[19] For example, in lithium-rich layered rock salt structures in which oxygen atoms are surrounded octahedrally by six cations, Figure 1, those that have linear Li–O–Li configurations are suggested to be linked to oxygen redox through the separation of hybridised oxygen 2p and transition metal 3d states.[5] In Na-deficient, Mn-based layered structures, two configurations of oxygen atoms have been identified, one containing OMn_3 units that do not contribute oxygen redox and one containing OMn_2 units that do contribute, by involving labile electrons in non-bonded O2p states just below the Fermi level.[10,20]

Our contention is that the key parameter that controls the onset of oxygen redox activity, at least during the first cycle of cathode charging, is the reduced amount of effective positive charge that surrounds some oxygen atoms in the crystal structure. If this is significantly less than $2+$, the oxide anions are underbonded and liable to oxidise; indeed, if underbonding is extreme, ionisation does not require an applied voltage and may be spontaneous.[12] This is because, as discussed later, the isolated O^{2-} ion is unstable in the gas phase; it is stabilised in the solid state only by the ionic lattice energies or covalent bond energies of the crystal structures.

Simple considerations of local electroneutrality, embodied in Pauling's original electrostatic bond strength ideas, highlight those structures and/or compositions in which some oxide ions may be underbonded. This leads to a generally-applicable and powerful criterion for rationalising oxygen redox and has the possibility to predict new redox-active materials. We illustrate the arguments involved with three sets of materials: (i) well-studied layered rock salt structures, both stoichiometric which are not oxygen redox-active and (ii) Li-rich[5] which are oxygen redox-active; (iii) $Li_4Mn_5O_{12}$, which is usually not considered as a possible cathode material, as it contains only Mn(IV), and was therefore believed to offer no charge compensation mechanism to facilitate delithiation during charging. However, anodic behaviour involving the Mn(IV)/Mn(III) redox couple is well established,[21] and is combined with its recently described oxygen redox behaviour in hybrid cation-oxygen-redox.[22,23] In reality, it can be difficult to identify whether transition metal cations or oxide ions are redox active under a certain set of conditions; often, both may be redox active simultaneously. For this reason, $Li_4Mn_5O_{12}$ is important as a test case, as discussed later.

Local Electroneutrality Considerations

Pauling's original local electroneutrality criterion for ionic structures considers the effective total cationic charge that surrounds a given oxygen atom in terms of the electrostatic bond strength, ebs, of each cation, given by its ratio: charge/coordination number CN. The requirement for local electroneutrality is given by:

$$\sum \text{ebs} = \sum \text{cation charge/cation CN} = +2$$

For high symmetry crystal structures such as those considered here, Pauling's criterion gives a good description of local structures and electroneutrality. For more complex, low symmetry structures that have variable cation-oxygen bond lengths, consideration of Brown's bond valence sum, bvs, criterion[24] may be more appropriate since this allows quantification of bond strength-bond length correlations. However, it then becomes more difficult to determine whether more complex structures do show residual departure from local electroneutrality or whether this is taken care of by application of the bvs model. Similarly, the oxygen bonding situation in highly covalent 4d and 5d metal oxides is probably beyond the scope of Pauling's description of ionic structures.

In the layered rock salt structures of stoichiometric $LiCoO_2$ and Li_2MnO_3 ($=Li[Li_{1/3}Mn_{2/3}O_2]$), the oxygen coordination environments are octahedral (OCo_3Li_3) and (OMn_2Li_4), respectively, Figure 1(a,b). Since each cation is octahedrally coordinated by oxygen, as CoO_6, MnO_6 and LiO_6 octahedra, the sum of the

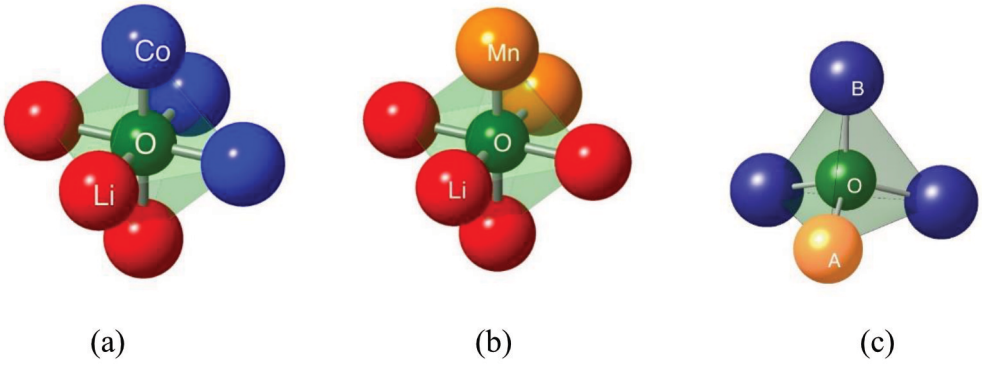

Figure 1. (a) octahedral OCo_3Li_3, (b) octahedral OMn_2Li_4, (c) tetrahedral $OA^{tet}B_3^{oct}$.

 © 2024 The Author(s). Zeitschrift für anorganische und allgemeine Chemie published by Wiley-VCH GmbH

15213749, 0, Downloaded from https://onlinelibrary.wiley.com/doi/10.1002/zaac.202400067 by UNIVERSITY OF SHEFFIELD, Wiley Online Library on [19/11/2024]. See the Terms and Conditions (https://onlinelibrary.wiley.com/terms-and-conditions) on Wiley Online Library for rules of use; OA articles are governed by the applicable Creative Commons License

electrostatic bond strengths around each oxygen atom, Σebs, is +2 for these stoichiometric structures and local electroneutrality holds. $LiCoO_2$ is redox-active by means of the $Co^{3+/4+}$ couple but stoichiometric Li_2MnO_3 containing Mn^{4+} is essentially inactive.[25] Although layered Li_2MnO_3 has been reported to undergo a phase transition into a disordered rock salt phase during high energy ball milling,[26] which would allow different ($OMn_{6-x}Li_x$) octahedra and consequently a variety of under- and overbonded oxygen atoms to be present, subsequent studies have highlighted the domain structure of some disordered rock salt compounds, which feature nano-domains that show a layered rock salt pattern and therefore, most octahedra are ($O_2Mn_2Li_4$).[27] However, the high surface area of nanomaterials such as these in which oxygen atoms do not have a full complement of surrounding cations, may be a source of underbonded oxygen atoms. Some underbonded oxygen atoms may also be present as the result of stacking faults, which are difficult to resolve by diffraction methods on nano-sized materials, but their abundance in Li_2MnO_3 is well documented by both transmission electron microscopy and electron diffraction,[28] and a link between their presence and enhanced oxygen redox behaviour is well established.[29,30] Computational studies yielded similar energies for different stacking sequences, explaining the abundance of stacking faults in Li_2MnO_3.[31]

Oxygen atoms in the spinel structure of $Li_4Mn_5O_{12}$ occupy tetrahedral sites with 4 cation neighbours, Figure 1(c); one of these neighbours is tetrahedrally coordinated to oxygen, the other three are octahedrally coordinated. The expanded structural formula may be written as $Li_3^{tet}(Li,Mn_5)^{oct}O_{12}$, consistent with the reported structure showing tetrahedral sites occupied by Li and octahedral sites occupied by a disordered mixture of Li and Mn.[32] It is not possible for any combination of Li^+ and Mn^{4+} ions distributed over three octahedral sites and Li^+ on one tetrahedral site to achieve local electroneutrality in this undistorted crystal structure; Σebs values for the different possibilities which are either underbonded or overbonded are $Li^{tet}Mn_3^{oct}$: +2.25, Li^{tet} ($Mn_2^{oct}Li^{oct}$): +1.75, Li^{tet} ($Mn^{oct}Li_2^{oct}$): +1.25 and $Li^{tet}Li_3^{oct}$: +0.75. The only electroneutral possibility would have Mn on the tetrahedral sites with $Mn^{tet}(Mn^{oct}Li_2^{oct})O_4$: +2.00.

Pauling's criterion is a very useful starting point for considering ionic crystal structures and possible departures from local electroneutrality. It has stood the test of time over many decades and has been a guiding principle for the description of ionic crystal structures.[33] Nevertheless, crystal structures such as $Li_4Mn_5O_{12}$ do exist in which possible departures from local electroneutrality must be taken into consideration. One way in which local electroneutrality could possibly be restored is if structural distortions leading to a range of cation-oxygen distances occur, and the structures could be tested using Brown's bvs criteria. However, there is no structural evidence of a lower symmetry structure or of local structural distortions in the high symmetry structure of cubic $Li_4Mn_5O_{12}$. This is also supported by excellent agreement between calculated and measured Kubo-Toyabe static muon depolarization rates, Δ, which implies no significant deviation of local bond lengths from those measured by diffraction.[34]

A second way in which local electroneutrality could possibly be restored involves back transfer of electron density from oxygen to high valence cations, such as observed in the charge transfer spectra under visible or UV radiation of permanganate species such as MnO_4^-. The occurrence of charge back transfer implies significant covalent bond formation between oxygen and the transition metal element which would reduce the underbonding on oxygen. However, this would also reduce the driving force for oxygen redox activity in the oxyanion species, consistent with the lack of examples of oxygen redox associated with oxyanions such as PO_4^{3-} in $LiFePO_4$.

$Li_4Mn_5O_{12}$ is not a particularly stable material and may be regarded as being on the edge of thermodynamic stability. It is believed to decompose above ~ 400 °C to give a mixture of a different spinel, $LiMn_2O_4$, and Li_2MnO_3.[32] Departure of the crystal structure from local electroneutrality may be associated with this limited thermodynamic stability and the emerging phenomenon of oxygen redox activity may be a direct consequence of this limited stability.

Similar arguments to the above may be applied to the well-studied, high capacity Li-rich layered rock salt structure oxides. These have formulae such as $Li_{1+x}(Mn,Ni,Co)_{1-x}O_2$ and many show a high level of oxygen redox activity in addition to that of the transition metal components.[5,35–37] Assuming that their structures are similar to that of $LiCoO_2$, the metal octahedra surrounding oxygen are undistorted ($OLi_{3+x}TM_{3-x}$). If x = 0, local electroneutrality holds, Figure 1(a). If x > 0, the average TM charge will be > 3+ and many of the octahedra cannot show local electroneutrality. For instance, in the octahedra ($OLi_4TM^{3+}TM^{4+}$), Σebs = +1.83 and ($OLi_4TM_2^{3+}$), Σebs = +1.67, whereas for ($OLi_3TM_2^{3+}TM_1^{4+}$), Σebs = +2.167 and ($OLi_3TM_1^{3+}TM_2^{4+}$), Σebs = +2.33. One octahedron does retain local electroneutrality, ($OLi_4TM_2^{4+}$), Σebs = +2 but this can represent only a small number of the octahedra.

Another established class of cathode materials that shows reversible oxygen redox is cation-deficient, layered $Na_{2/3}[Mg_{1/3}Mn_{2/3}]O_2$-type materials,[38] in which cation vacancies in the Na layer will, applying the same principle as outlined above, allow for an even wider distribution of local deviations from electroneutrality. The logical conclusion, therefore, is that the non-stoichiometry and local structure of high symmetry layered rock salt materials leads inevitably to a large number of oxygen atoms that may be underbonded. Several studies have shown that high capacity lithium-rich layered rock salt structure materials undergo three processes on first charge. First is oxidation of the transition metals to the 4+ state. Second is characterised by a 4.5 V plateau attributed to first step oxidation of oxygen O^{2-} and presumably formation of the O^- state, without oxygen release. Third, at even higher voltages, the second oxygen oxidation step leads to the release of O_2 gas. Remarkably, the main cation in these materials is Mn^{4+} but it takes little part in the redox reactions which instead involve a combination of oxygen and the other transition elements.

The literature contains numerous reports on the synthesis, structure and properties of $Li_4Mn_5O_{12}$[39] and especially, Li_2MnO_3.[40] We report here confirmatory studies on Li_2MnO_3 and

 © 2024 The Author(s). Zeitschrift für anorganische und allgemeine Chemie published by Wiley-VCH GmbH

15213749, 0, Downloaded from https://onlinelibrary.wiley.com/doi/10.1002/zaac.202400067 by UNIVERSITY OF SHEFFIELD, Wiley Online Library on [19/11/2024]. See the Terms and Conditions (https://onlinelibrary.wiley.com/terms-and-conditions) on Wiley Online Library for rules of use; OA articles are governed by the applicable Creative Commons License

additional structural, thermodynamic and magnetic characterisation measurements on $Li_4Mn_5O_{12}$.

Experimental

Li_2MnO_3 with layered rock salt structure was made by solid-state synthesis. Li_2CO_3 (Sigma Aldrich, 99%) and MnO (Sigma Aldrich, 99%) were weighed in stoichiometric amounts to give a 5 g sample and hand ground with pestle and mortar facilitated by addition of a few drops of acetone. The reaction mixtures were filled in corundum crucibles, transferred to a muffle furnace and heated to 400 °C at a rate of 5 °C/min, kept at temperature for 12 h for calcination and allowed to cool naturally. The resulting powders were reground with a pestle and mortar, filled in corundum crucibles, transferred to a muffle furnace and heated to 800 °C at a rate of 5 °C/min, kept at temperature for 36 h for reaction to complete and then allowed to cool naturally.

Li_2MnO_3 with disordered rock salt structure and $Li_4Mn_5O_{12}$ were both prepared by mechanosynthesis. Li_2O (Sigma Aldrich, 95%) and MnO_2 (Sigma Aldrich, 99%) were weighed in the respective stoichiometric ratios to give a total sample mass of 3 g and filled in 20 ml zirconia ball milling jars containing 10 zirconia balls of 10 mm diameter. The mechanosynthesis was performed in a Fritsch P7 planetary ball mill for 16 cycles of milling at 750 rpm for 1 h each, followed by a rest period of 5 min between cycles.

X-ray diffraction was performed on a STOE STADI P diffractometer (Darmstadt, Germany) operated in transmission mode with a MYTHEN strip detector and a Ge monochromator. The diffractometer was operated at 45 kV and 45 mA using Mo $K\alpha_1$ radiation, $\lambda =$ 0.7090 Å. The scan range was $2\theta = 4$–$60°$ with a step size of 1.5° and count time of 70 s. Samples were prepared by hand grinding the powder by pestle and mortar and finely distributing it between two discs of acetate film mounted on a specimen holder.

Powder neutron diffraction patterns were collected in Banks 1–5 of the Polaris instrument[41] at the ISIS pulsed neutron and muon source at the Rutherford Appleton Laboratory, UK. Around 3 g of finely ground $Li_4Mn_5O_{12}$ powder was loaded into a cylindrical vanadium can (diameter: 11 mm). The data were collected at room temperature over a time-of-flight region 0.25–23 ms.

Rietveld refinements of combined X-ray data and neutron data were performed using GSAS-II.[42] The instrument parameter file of STOE was obtained by careful refinement of the XRD pattern of LaB_6 standard collected before the measurement of the samples; instrument parameter file of Polaris was offered by ISIS.

The DC magnetic susceptibility was measured as a function of temperature on a Quantum Design MPMS 3 magnetometer. Finely ground, polycrystalline samples (about 20 mg) were mounted in a gelatine capsule. After cooling from room temperature to 4 K without applied magnetic field, a field $H = 1000$ G was applied and the zero field cooled (ZFC) DC magnetisation measured as a function of temperature during heating to room temperature. Subsequently, the sample was cooled back to 4 K while applying a magnetic field $H = 1000$ G, and the field cooled (FC) DC magnetisation measured as a function of temperature during heating to room temperature.

Thermogravimetric analysis was performed using a SETSYS instrument (Setaram, France). Around 50 mg of sample was used for each measurement, while the atmosphere needed was set to flow at 40 ml/min. Samples were stored prior to use either in a desiccator or a glove box, then heated/cooled at 5 K/min during the procedure.

For electrochemical testing, each Li–Mn–O composition was mixed separately with polyvinylidene fluoride (PVDF) binder (Solvay) and C65 carbon black conductive additive (Imerys) in an 8:1:1 ratio. Uniform slurries were formed with N-methyl-2-pyrrolidone (NMP) (Sigma Aldrich) using a THINKY ARE-250 non-contact planetary mixer. Each slurry was drawn down onto carbon-coated Al foil (MTI), dried and stored in an 80 °C vacuum oven. Once dry, 12 mm diameter electrodes were punched from the foil and used for cell preparation. Electrochemical experiments were performed using CES 2032-type coin cells with a Whatman glass fibre separator and 16 mm lithium chip (CES) as the counter electrode. The electrolyte was 1 M $LiPF_6$ in a 3:7 solution of ethylene carbonate (EC) and ethyl methyl carbonate (EMC) (Solvionic). The cells were assembled in an argon-filled glove box (MBraun) with oxygen and water contents less than 0.1 ppm. Electrochemical cycling was performed using a Maccor Series 4000 Automated Test System. All cells were held at a constant temperature of 25 ± 0.5 °C. Each cell was left for 8 h at 25 °C prior to cycling to allow time to equilibrate. The cells were charged and discharged at 15 mA g^{-1}, in a voltage window of 2–4.7 V. At 4.7 V, a 30 minute constant voltage step was used to complete the charging process.

Results and Discussion

Electrochemical Properties

We illustrate the effect of underbonded oxygen atoms on electrochemical properties by the contrasting behaviour as cathode materials of two standard lithium manganese oxides, Li_2MnO_3 and $Li_4Mn_5O_{12}$, and in particular by the confirmation that $Li_4Mn_5O_{12}$ is, unexpectedly, a reversible high capacity cathode.[22,23,43–45] Their crystal structures are very similar - layered rock salt and spinel, respectively - and are both based on cubic close packed oxide ions but with cations distributed rather differently over the available tetrahedral and octahedral sites. Because both structures contain Mn^{4+} cations, neither would be expected to show much redox activity as cathodes. This is indeed the case for well-ordered, monoclinic Li_2MnO_3.[46–49] When prepared by high temperature solid state reaction, Figure 2, it shows only a small charge-discharge capacity, Figure 3(a), on repeated cycling, as expected. Similarly, when prepared by mechanosynthesis as a cubic disordered rock salt structure, Figure 2, its reversible charge-discharge capacity is small, Figure 3(b) and further illustrates that stoichiometric Li_2MnO_3 offers little possibility as a cathode. In agreement with the literature, layered Li_2MnO_3 shows an initial irreversible first charge capacity larger than that of disordered Li_2MnO_3.[26] and is attributed to oxygen loss and surface rearrangement to from a MnO_2-shell around a Li_2MnO_3 core.[50] Mechanosynthesised disordered Li_2MnO_3 is believed to show surface densification by disproportionation reaction to $Li_{2-x}MnO_3$ and Li_2O, with the latter regarded as the actual redox active component.[27]

There are reports of high redox activity of nano-Li_2MnO_3 prepared by high energy ball milling,[26,27,51] but also evidence that in some cases, the products are oxygen-deficient, such as $Li_2MnO_{2.5}$,[52,53] leading to redox-active Mn^{3+} ions. In our materials, there is no evidence that nano-Li_2MnO_3 made by either mechanosynthesis, or by ball milling ordered Li_2MnO_3 initially made by solid-state synthesis, is oxygen-deficient. The

 © 2024 The Author(s). Zeitschrift für anorganische und allgemeine Chemie published by Wiley-VCH GmbH

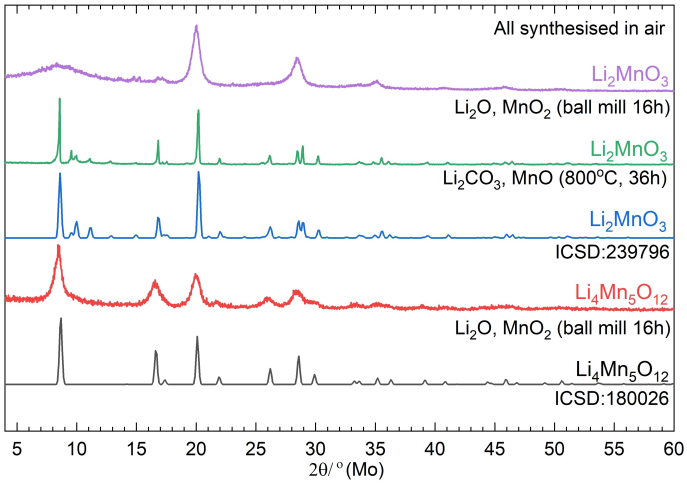

Figure 2. XRD patterns of Li_2MnO_3 and $Li_4Mn_5O_{12}$ synthesised via different routes.

reversible capacities of Li_2MnO_3 made by either mechanosynthesis or high temperature solid state reaction followed by ball milling are small, Figure 3(a,b), which is an indication that the materials are oxygen stoichiometric and do not contain significant amounts of Mn^{3+} ions. The small residual capacity that is observed could be variously associated with a small oxygen deficiency and the presence of Mn^{3+} ions, or under-bonded oxygen atoms in either the surface structure, at nano-domain interfaces[27] or stacking faults.[30]

$Li_4Mn_5O_{12}$ was prepared by mechanosynthesis at room temperature as nano-sized particles, Figure 2. The spinel structure and composition was confirmed by Rietveld refinement of combined powder X-ray and neutron diffraction data, Table 1 and Figure 4. The Li:Mn cation ratio was close to the expected (Table 1b), and was hence fixed to allow for a stable and reliable refinement of isotropic atomic displacement parameters, Uiso; full occupancy of the oxygen sites was confirmed, Table 1(a). This is important as it confirms, indirectly, that Mn was present solely as Mn^{4+}. Because of its formula, $Li_4Mn_5O_{12}$ does not fall simply into the 'normal/inverse' spinel categories. The tendency is for it to adopt a 'normal' structure with Li in tetrahedral sites and Mn in octahedral sites, but the excess Li that is present beyond the usual spinel stoichiometry is disordered with Mn over the octahedral sites.

The results of our DC magnetometry study, Figure 5, corroborate these findings. The material shows Curie-Weiss behaviour at high temperatures (150–300 K), and the ZFC inverse molar magnetic susceptibility χ_{mol}^{-1} was well described by the Curie-Weiss law with a Curie-Weiss temperature $\theta_{CW} = -58.4(3)$ K and a Curie constant $C = 1.934(3)$ emu mol^{-1} K^{-1}. The latter corresponds to an experimentally determined effective magnetic moment of $\mu_{eff.}^{exp.} = 3.93\,\mu_B$, which agrees very well with the value obtained for a $3d^3$ spin-only model, $\mu_{eff.}^{cal.} = 3.88\,\mu_B$, thereby implying that the vast majority of manganese species are Mn^{4+}.

$Li_4Mn_5O_{12}$ is not a stable high temperature material but is reported to decompose above about 400 °C to give a mixture of the spinel $LiMn_2O_4$ and Li_2MnO_3.[54] This lack of thermal stability is confirmed by preliminary thermogravimetry results, Figure 6 of a sample heated at 5 °C min^{-1} in N_2. The sample starts to lose weight gradually soon above room temperature and weight loss continues to at least 700 °C. Work is in progress to characterise the decomposition products and compare the weight loss profile in different atmospheres. Care is clearly required to avoid, and be aware of, this decomposition because the XRD pattern of $LiMn_2O_4$ spinel is very similar to that of $Li_4Mn_5O_{12}$ and $LiMn_2O_4$ contains Mn^{3+} which is redox-active.

Electrochemical results on $Li_4Mn_5O_{12}$ are shown in Figure 7 and are similar in general appearance to those reported previously.[22] Cycling over the range 3–4.7 V (a,b) shows a reversible cathodic process with capacity 84 mAh g^{-1} that is attributed to oxygen redox based on the O^{2-}/O^{-} couple. The reversibility indicates that the second step of oxygen redox and evolution of O_2 gas does not occur. We have no direct spectroscopic evidence to discount the possibility of Mn^{4+} oxidation during charging above 3 V but note that there has not been any strong evidence of Mn^{4+} oxidation in the literature on Mn-based materials.

Table 1. Refinement of combined X-ray and neutron diffraction data on mechano-synthesized $Li_4Mn_5O_{12}$ in space group F m −3 m, a = 8.1325(6) Å, $\chi^2 = 7.29$, wR = 4.661 % (a) Uiso refinement only, constraint of Uiso(Li1) = Uiso(Li2) applied; (b) Cation fraction and oxygen position refinement based on fixed Uisos; constraint of fraction(Li2) + fraction(Mn1) = 1 applied.

(a)

label	elem	mult	x	y	z	frac	Uiso
Li1	Li^+	8	0.125	0.125	0.125	1.000	**0.021(1)**
Li2	Li^+	16	0.5	0.5	0.5	0.150	**0.021(1)**
Mn1	Mn^{4+}	16	0.5	0.5	0.5	0.850	**0.00916(3)**
O1	O^{2-}	32	0.262578	0.262578	0.262578	1.000	**0.00100(1)**

(b)

label	elem	mult	x	y	z	frac	Uiso
Li1	Li^+	8	0.125	0.125	0.125	**0.941(25)**	0.021
Li2	Li^+	16	0.5	0.5	0.5	**0.170(9)**	0.021
Mn1	Mn^{4+}	16	0.5	0.5	0.5	**0.830(9)**	0.0092
O1	O^{2-}	32	**0.26256(4)**	**0.26256(4)**	**0.26256(4)**	1.000	0.001

© 2024 The Author(s). Zeitschrift für anorganische und allgemeine Chemie published by Wiley-VCH GmbH

15213749, 0, Downloaded from https://onlinelibrary.wiley.com/doi/10.1002/zaac.202400067 by UNIVERSITY OF SHEFFIELD, Wiley Online Library on [19/11/2024]. See the Terms and Conditions (https://onlinelibrary.wiley.com/terms-and-conditions) on Wiley Online Library for rules of use; OA articles are governed by the applicable Creative Commons License

15213749, 0, Downloaded from https://onlinelibrary.wiley.com/doi/10.1002/zaac.202400067 by UNIVERSITY OF SHEFFIELD, Wiley Online Library on [19/11/2024]. See the Terms and Conditions (https://onlinelibrary.wiley.com/terms-and-conditions) on Wiley Online Library for rules of use; OA articles are governed by the applicable Creative Commons License

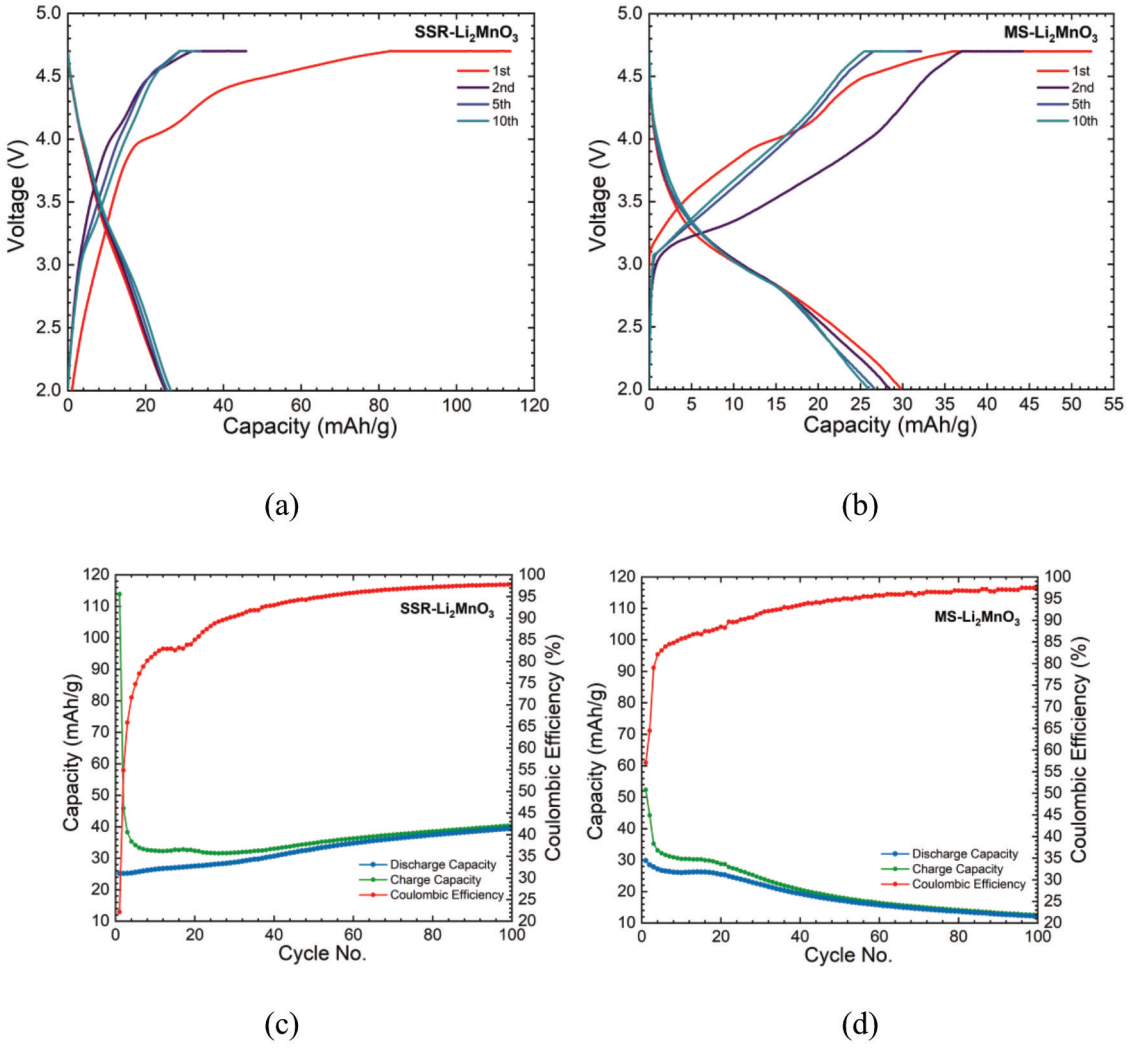

Figure 3. Charge/discharge curves for (a) solid-state synthesized, (b) mechano-synthesized Li_2MnO_3 vs. lithium in 2–4.7 V range at a rate of 15 mA/g; coulombic efficiency and capacity vs. cycle number for (c) solid-state synthesized, (d) mechano-synthesized Li_2MnO_3.

Subsequent cycling over the range 2–4.7 V shows both the high voltage cathodic process and also anodic insertion of Li below 3 V associated with the Mn^{4+}/Mn^{3+} couple. The anodic capacity is cycle-dependent and gradually decreases from an initial value of about 80 mAh g^{-1}. The overall Coulombic efficiency is high (97%) over 100 cycles, apart from the anomalous first half cycle, during which the total discharge capacity exceeds the observed charge capacity due to the pristine material being only partially lithiated and the true columbic efficiency cannot be calculated simply from the measured capacities. The capacities show a gradual decrease on cycling from 174–110 mAh g^{-1}.

It is proposed that the higher voltage cathodic results which are attributed to redox-active oxygen are associated with the presence of underbonded oxygen atoms in the spinel crystal structure of $Li_4Mn_5O_{12}$. The difference in profiles between the first and subsequent cycles on charging above 3 V, indicates possible structural changes on the first cycle; however, the high reversibility on cycling, Figure 7(b) indicates that oxidation of O^{2-} is limited to one-electron step. The anodic behaviour of $Li_4Mn_5O_{12}$[21] is similar to that of $Li_4Ti_5O_{12}$, which behaves as an anode in its charged state, $Li_7Ti_5O_{12}$ and contains mixed valence $Ti^{3+/4+}$.[55]

Underbonded Oxide Ions and Redox Activity

The next question to be addressed is: why are underbonded oxide ions able to ionise readily, but those in electrically neutral environments are not? The answer comes from the well-known

 © 2024 The Author(s). Zeitschrift für anorganische und allgemeine Chemie published by Wiley-VCH GmbH

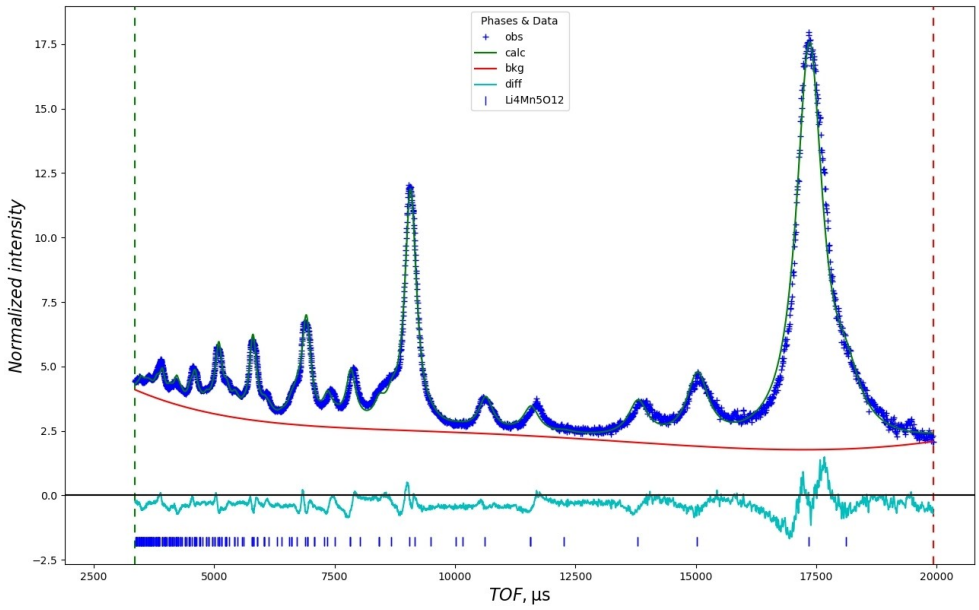

Figure 4. Rietveld refinement of mechano-synthesized $Li_4Mn_5O_{12}$ using combined neutron and XRD data.

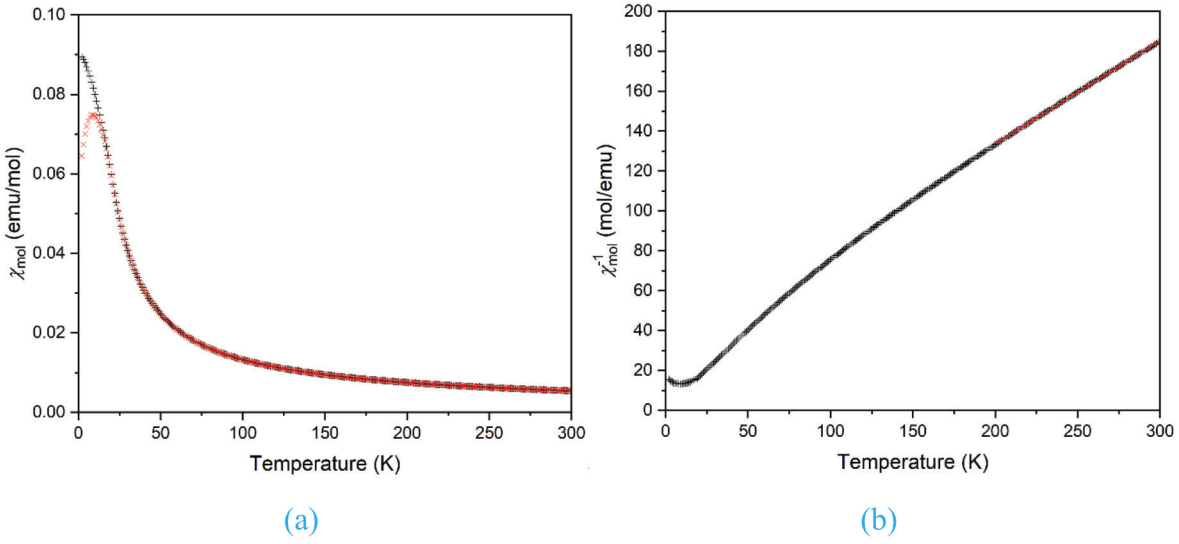

Figure 5. a) *DC* susceptibility χ_{mol} of $Li_4Mn_5O_{12}$ (applied field $H = 1000$ G) for ZFC (+) and FC (x) magnetometry. b) Inverse *DC* susceptibility χ_{mol}^{-1}. The red solid line shows a fit to the Curie-Weiss law for $T \geq 200$ K, with the parameter $C = 1.934(3)$ emu mol^{-1} K^{-1} and a Curie-Weiss temperature, $\theta_{CW} = -58.4(3)$ K.

fact that the oxide ion, O^{2-}, is spontaneously unstable in the gas phase and should ionise to give $O^- + e^-$.[12] This does not readily happen in crystal lattices because the O^{2-} ion is stabilised either by the higher lattice energy of ionic crystal structures built of divalent oxide ions than that of (hypothetical) crystal structures built of monovalent O^- ions or by the strong covalent bonds formed by O in combination with high valency cations. Consequently, there has never been any serious suggestion that crystal structures built of O^- ions could exist (although structures built of peroxide, O_2^{2-} and superoxide, O_2^- do, of course, exist), because more stable crystal structures built of O^{2-} ions or covalently-bonded O atoms are always preferred energetically.

Underbonded oxide ions represent a situation of intermediate stability since they are not surrounded by a full complement of positive charge. This may lead to various levels of destabilisation of the O^{2-} ion and a decrease in its first ionisation potential; in extreme cases, this stabilisation may become zero leading to spontaneous oxidation, as observed in the *p*-type behaviour of acceptor-doped titanate ceramics.[12] Three situations may be

© 2024 The Author(s). Zeitschrift für anorganische und allgemeine Chemie published by Wiley-VCH GmbH

15213749, 0, Downloaded from https://onlinelibrary.wiley.com/doi/10.1002/zaac.202400067 by UNIVERSITY OF SHEFFIELD, Wiley Online Library on [19/11/2024]. See the Terms and Conditions (https://onlinelibrary.wiley.com/terms-and-conditions) on Wiley Online Library for rules of use; OA articles are governed by the applicable Creative Commons License

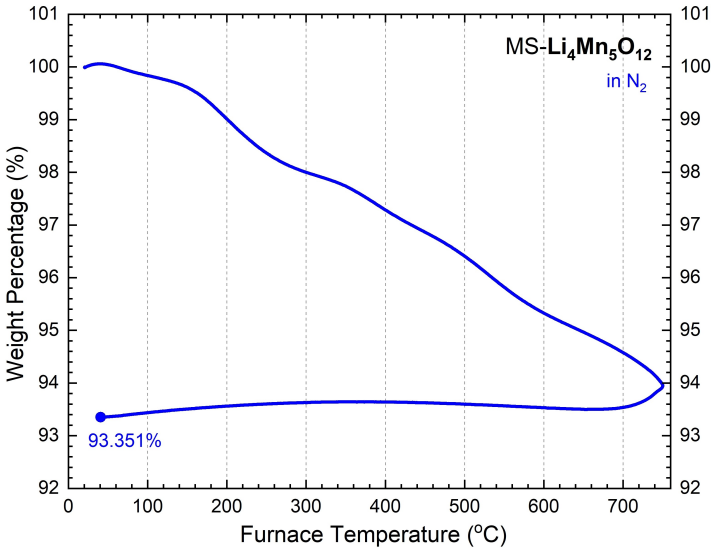

Figure 6. TGA plot of mechano-synthesized $Li_4Mn_5O_{12}$

envisaged in which oxide ions in regular oxide lattices are underbonded:

First, in acceptor-doped crystal structures in which a cation of a parent structure is substituted by a cation of lower charge, as in Mg-doped $BaTiO_3$, $BaTi_{1-x}Mg_xO_{3-x}$. Oxygen atoms that have one Ti atom substituted by Mg in its first coordination shell experience reduced total positive charge, which leads to the relatively easy first oxidation of those oxide ions and creation of holes on oxygen that are responsible for *p*-type conductivity.[56] Such *p*-type conductivity associated with electron holes appears to be commonplace in many acceptor-doped oxides, especially those whose defect structure contains oxygen vacancies which are able to absorb oxygen from the atmosphere, dissociate and ionise to give O^- ions.

Second, many oxide ions are coordinatively unsaturated at the surface, for instance those in the outer (222) layer of rock salt structured oxides, which can be a layer of either oxide anions or metal cations. This may account for the common observation of oxidised oxygen species such as peroxide O_2^{2-}, superoxide O_2^- and O^- anions in surface science studies, although these are not found to the same extent in sample interiors.[57]

Third, in materials such as stoichiometric $Li_4Mn_5O_{12}$ which have high symmetry cubic structures, some of the oxide ions are inevitably underbonded and cannot avoid departures from local electroneutrality. Compositional constraints mean that the structure around an oxygen site is an average of several contributing local structures; some of these are underbonded and others are overbonded. The family of Li-rich layered rock salt solid solutions of general formula $Li_{1+x}TM_{1-x}O_2$ contains several high capacity cathodes which have a significant redox-active oxygen contribution. As discussed above for $x>0$, the average TM charge will be $>+3$ which ideally, leads to a mixture of underbonded and overbonded oxygen atoms, depending on their immediate cation environment. A similar situation of locally under- and overbonded oxygen atoms may arise in stoichiometric layered rock salt oxides that exhibit a degree of cation disorder, whether it be antisite defects in truly stoichiometric compounds, or a small amount of reduced transition metal ions in the Li layer due to slight Li deficiency in compounds like $Li_{1+/-x}NiO_2$, which is notoriously difficult to synthesise for $x=0$ as the temperature ranges of crystallisation and decomposition overlap.[58]

The link between underbonded oxide ions and their redox activity has previously not been recognised explicitly for its involvement with high capacity cathodes, although there is widespread acknowledgement that during charging, holes may be created by oxidation of O^{2-} ions.[59] The focus of this publication is on the nature of oxygen species in pristine condition materials. Most of the discussions in the literature concern their nature in the charged state, in which holes created during charging are located on oxygen but the nature of the resulting oxygen species is still a matter of debate.[3,5,9,11,60] It has been suggested variously that: the holes may be localised[59] or delocalized;[11] catenated species such as O_2^{2-}, O_2^- or other peroxo species may form[60,61]; in the absence of direct evidence, non-specific species O^{n-} have been labelled.[3,62] We have no direct spectroscopic evidence for the nature of the oxygen species involved, but since anionic redox processes must always be initiated by a hole localised on the anion,[63] it is, for present purposes, sufficient to refer to them simply as O^- ions.

Conclusions

Very few stoichiometric crystal structures show significant departures from Pauling's local electroneutrality criterion. The only example of which we are aware is the spinel $Li_4Mn_5O_{12}$ (and analogues such as $Li_4Ti_5O_{12}$). This spinel is neither normal

© 2024 The Author(s). Zeitschrift für anorganische und allgemeine Chemie published by Wiley-VCH GmbH

15213749, 0, Downloaded from https://onlinelibrary.wiley.com/doi/10.1002/zaac.202400067 by UNIVERSITY OF SHEFFIELD, Wiley Online Library on [19/11/2024]. See the Terms and Conditions (https://onlinelibrary.wiley.com/terms-and-conditions) on Wiley Online Library for rules of use; OA articles are governed by the applicable Creative Commons License

15213749, 0, Downloaded from https://onlinelibrary.wiley.com/doi/10.1002/zaac.202400067 by UNIVERSITY OF SHEFFIELD, Wiley Online Library on [19/11/2024]. See the Terms and Conditions (https://onlinelibrary.wiley.com/terms-and-conditions) on Wiley Online Library for rules of use; OA articles are governed by the applicable Creative Commons License

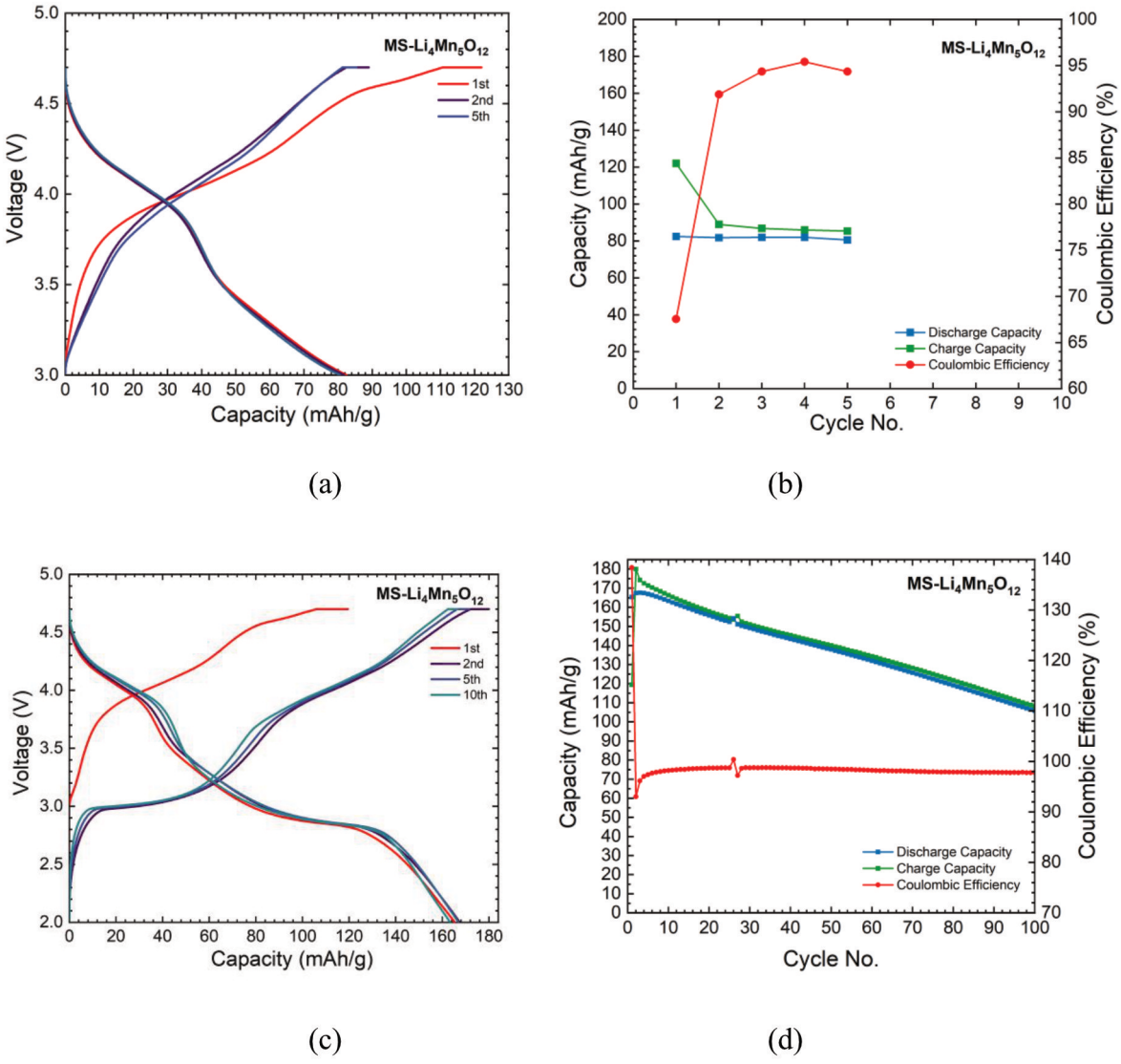

Figure 7. (a) Charge/discharge curves for mechano-synthesized $Li_4Mn_5O_{12}$ vs. lithium in 3–4.7 V range at 15 mA/g with (b) coulombic efficiency and capacity vs. cycle number; (c) charge/discharge curves in 2–4.7 V range at 15 mA/g with (d) coulombic efficiency and capacity vs. cycle number.

nor inverse. A combination of local structural and compositional constraints causes it to have significant departures from local electroneutrality which lead to a distribution of under- and overbonded oxygen atoms. There is no experimental evidence of structural distortions or lower symmetry local structures that could reduce the departure from local electroneutrality. For more complex, lower symmetry structures, Brown's bond valence calculations are usually used to rationalise possible departures from local electroneutrality.

Departures from local electroneutrality may occur widely in non-stoichiometric materials such as the Li-rich layered rock salt materials, and defective, sub-stoichiometric materials such as $Li_{1+/-x}NiO_2$ in which lithium loss involves displacement of the generated Ni^{2+} ions into the Li layers.

Oxide ions, O^{2-} are spontaneously unstable in the gas phase but are usually fully stabilised in the solid state by the lattice energy of crystal structures: each oxide ion is surrounded by an effective positive charge of $2+$. Underbonded oxygen atoms that are not surrounded by a full complement of cation charge have reduced stabilisation, are readily oxidised and appear to be the source of oxygen redox processes in cathode materials such as $Li_4Mn_5O_{12}$ and Li-rich layered rock salt materials.

$Li_4Mn_5O_{12}$ shows a clear separation of redox-active oxygen and cathodic behaviour above 3 V from redox-active Mn and anodic behaviour below 3 V. Although a similar separation is found for highly covalent model compounds like $Li_{2+x}MO_{3+x}$ (M=Ru, Ir),[64–66] this is, to the authors knowledge, the first example of a practical material featuring solely earth-abundant

 © 2024 The Author(s). Zeitschrift für anorganische und allgemeine Chemie published by Wiley-VCH GmbH

15213749, 0, Downloaded from https://onlinelibrary.wiley.com/doi/10.1002/zaac.202400067 by UNIVERSITY OF SHEFFIELD, Wiley Online Library on [19/11/2024]. See the Terms and Conditions (https://onlinelibrary.wiley.com/terms-and-conditions) on Wiley Online Library for rules of use; OA articles are governed by the applicable Creative Commons License

3d metal elements in which oxygen redox is clearly separable from cation redox. The high reversibility of the anion redox indicates that in this case, oxidation of O^{2-} ions is a one-electron process, which is highly desirable for application possibilities that must avoid O_2 loss during cycling. The oxygen atoms in $Li_4Mn_5O_{12}$ are tetrahedrally coordinated and the possibility of linear Li–O–Li units with O in octahedral coordination being responsible for the oxygen redox activity can be excluded.

Use of electrostatic bond strength ideas does not require that the structures are ideally ionic since most bonds are of mixed ionic-covalent character. But a combination of valence bond theory and ionic bonding ideas demonstrates that either departures from local electroneutrality are present, or other structural/bonding changes would be required to regain local electroneutrality. The simple approach used here has powerful predictive possibilities, can rationalise which structures may show underbonded oxygen atoms and thereby, suggest a direct link to possible oxygen redox activity.

Author Contributions

YZ and XZ: sample preparation; YZ: XRD, TGA; YZ and LM: electrochemical measurements; PG: magnetometry, neutron diffraction; YZ and PG: Rietveld refinement, discussion of results and manuscript preparation; ARW: conceived and supervised the overall project, prepared first draft of manuscript. All authors contributed to and approved the final version.

Acknowledgements

This work was supported by The Faraday Institution grant number FIRG017 and EPSRC grant number EP/X040305/1. The ISIS Neutron and Muon Source is acknowledged for beamtime on Polaris (https://doi.org/10.5286/ISIS.E.RB2200305#).

Conflict of Interests

The authors declare no competing interests.

Data Availability Statement

The data that support the findings of this study are available from the corresponding author upon reasonable request.

[1] Z. Lu, J. R. Dahn, *J. Electrochem. Soc.* **2002**, *149*, A815, https://doi.org:10.1149/1.1480014.
[2] M. D. Radin, J. Vinckeviciute, R. Seshadri, A. Van Der Ven, *Nat. Energy* **2019**, *4*, 639–646, https://doi.org:10.1038/s41560-019-0439-6.
[3] G. Assat, J.-M. Tarascon, *Nat. Energy* **2018**, *3*, 373–386, https://doi.org:10.1038/s41560-018-0097-0.
[4] J. Zhang, et al., *J. Am. Chem. Soc.* **2023**, *145*, 10208–10219, https://doi.org:10.1021/jacs.3c01128.
[5] D.-H. Seo, et al., *Nat. Chem.* **2016**, *8*, 692–697, https://doi.org:10.1038/nchem.2524.
[6] Q. Wu, et al., *Energy Fuels* **2022**, *36*, 8081–8095https://doi.org:10.1021/acs.energyfuels.2c01601.
[7] Z. Lun, et al., *Nat. Mater.* **2021**, *20*, 214–221, https://doi.org:10.1038/s41563-020-00816-0.
[8] T. Liu, et al., *Nature* **2022**, *606*, 305–312, https://doi.org:10.1038/s41586-022-04689-y.
[9] R. A. House, et al., *Nat. Energy* **2021**, *6*, 781–789, https://doi.org:10.1038/s41560-021-00780-2.
[10] R. A. House, et al., *Nature* **2020**, *577*, 502–508, https://doi.org:10.1038/s41586-019-1854-3.
[11] R. A. House, et al., *Nat. Energy* **2023**, *8*, 351–360, https://doi.org:10.1038/s41560-023-01211-0.
[12] A. R. West, *J. Mater. Chem. A* **2023**, *11*, 12681–12694, https://doi.org:10.1039/d3ta00202k.
[13] R. Jung, M. Metzger, F. Maglia, C. Stinner, H. A. Gasteiger, *J. Electrochem. Soc.* **2017**, *164*, A1361–A1377, https://doi.org:10.1149/2.0021707jes.
[14] H. Koga, et al., *J. Phys. Chem. C* **2014**, *118*, 5700–5709, https://doi.org:10.1021/jp412197z.
[15] H. Koga, et al., *J. Power Sources* **2013**, *236*, 250–258, https://doi.org:https://doi.org/10.1016/j.jpowsour.2013.02.075.
[16] K. McColl, et al., *Nat. Commun.* **2022**, *13*, https://doi.org:10.1038/s41467-022-32983-w.
[17] K. Hoang, *Phys. Rev. Appl.* **2015**, *3*, https://doi.org:10.1103/physrevapplied.3.024013.
[18] A. M. Abakumov, S. S. Fedotov, E. V. Antipov, J.-M. Tarascon, *Nat. Commun.* **2020**, *11*, 4976.
[19] N. Yabuuchi, et al., *Nat. Commun.* **2016**, *7*, 13814, https://doi.org:10.1038/ncomms13814.
[20] H. Hafiz, et al., *Nature* **2021**, *594*, 213–216, https://doi.org:10.1038/s41586-021-03509-z.
[21] M. M. Thackeray, et al., *J. Electrochem. Soc.* **1992**, *139*, 363, https://doi.org:10.1149/1.2069222.
[22] Y. Liu, et al., *Chem. Commun.* **2019**, *55*, 8118–8121, https://doi.org:10.1039/c9cc02006c.
[23] R. N. Zhu, J. Wang, J. Li, *Chem. Res. Chin. Univ.* **2021**, *37*, 1031–1043, https://doi.org:10.1007/s40242-021-1305-1.
[24] I. D. Brown, *Acta. Crystallogr. B* **1977**, *33*, 1305–1310, https://doi.org:10.1107/S0567740877005998.
[25] J. G. Yang, Y. B. Niu, X. Wang, M. W. Xu, *Inorg. Chem. Front.* **2021**, *8*, 4300–4312, https://doi.org:10.1039/d1qi00687h.
[26] M. Freire, O. I. Lebedev, A. Maignan, C. Jordy, V. Pralong, *J. Mater. Chem. A* **2017**, *5*, 21898–21902, https://doi.org:10.1039/c7ta07476j.
[27] M. Diaz-Lopez, et al., *J. Mater. Chem. A* **2020**, *8*, 10998–11010, https://doi.org:10.1039/d0ta03372c.
[28] A. Boulineau, L. Croguennec, C. Delmas, F. Weill, *Chem. Mater.* **2009**, *21*, 4216–4222, https://doi.org:10.1021/cm900998n.
[29] X. Li, et al., *Adv. Energy Mater.* **2022**, *12*, 2200427, https://doi.org:https://doi.org/10.1002/aenm.202200427.
[30] B. Wang, et al., *Adv. Mater.* **2023**, *35*, 2207904, https://doi.org:10.1002/adma.202207904.
[31] Y. Koyama, I. Tanaka, M. Nagao, R. Kanno, *J. Power Sources* **2009**, *189*, 798–801, https://doi.org: 10.1016/j.jpowsour.2008.07.073.
[32] T. Takada, H. Hayakawa, E. Akiba, *J. Solid State Chem.* **1995**, *115*, 420–426, https://doi.org:10.1006/jssc.1995.1154.
[33] L. Pauling, *The Nature of the Chemical Bond and the Structure of Molecules and Crystals; an Introduction to Modern Structural Chemistry*, Cornell University Press, Oxford University Press, H. Milford **1939**.

 © 2024 The Author(s). Zeitschrift für anorganische und allgemeine Chemie published by Wiley-VCH GmbH

[34] M. J. Ariza, D. J. Jones, J. Rozière, J. S. Lord, D. Ravot, *J. Phys. Chem. B* **2003**, *107*, 6003–6011, https://doi.org:10.1021/jp027022n.
[35] J. Xu, et al., *Nat. Commun* **2018**, *9*, https://doi.org:10.1038/s41467-018-03403-9.
[36] B. Li, et al., *Nat. Mater.* **2023**, *22*, 1370–1379, https://doi.org:10.1038/s41563-023-01679-x.
[37] A. S. Menon, et al., *PRX* Energy **2023**, *2*, https://doi.org:10.1103/prxenergy.2.013005.
[38] N. Yabuuchi, et al., *J. Mater. Chem. A* **2014**, *2*, 16851–16855, https://doi.org:10.1039/C4TA04351K.
[39] C. Masquelier, et al., *J. Solid State Chem.* **1996**, *123*, 255–266, https://doi.org: 10.1006/jssc.1996.0176.
[40] D. L. Ye, L. Z. Wang, *Mater. Technol.* **2014**, *29*, A59–A69, https://doi.org:10.1179/1753555714Y.0000000166.
[41] R. I. Smith, et al., *Rev. Sci. Instrum* **2019**, *90*, https://doi.org:10.1063/1.5099568.
[42] B. H. Toby, R. B. Von Dreele, *J. Appl. Crystallogr.* **2013**, *46*, 544–549, https://doi.org:10.1107/S0021889813003531.
[43] X. J. Gu, Y. J. Cai, X. Yao, H. L. Tian, Z. Su, *New J. Chem.* **2022**, *46*, 21350–21355, https://doi.org:10.1039/d2nj03731a.
[44] Y. M. Huang, et al., *Adv. Energy Mater.* **2021**, *11*, https://doi.org:10.1002/aenm.202000997.
[45] S. Li, et al., *Nano Lett.* **2021**, *21*, 4176–4184, https://doi.org:10.1021/acs.nanolett.0c04920.
[46] X. Bian, et al., *Chem. Mater.* **2015**, *27*, 5745–5754, https://doi.org:10.1021/acs.chemmater.5b02331.
[47] M. Gu, et al., *ACS Nano* **2013**, *7*, 760–767, https://doi.org:10.1021/nn305065u.
[48] C. Ghanty, R. N. Basu, S. B. Majumder, *Solid State Ion.* **2014**, *256*, 19–28, https://doi.org:10.1016/j.ssi.2013.12.032.
[49] S. H. Park, Y. Sato, J. K. Kim, Y. S. Lee, *Mater. Chem. Phys.* **2007**, *102*, 225–230, https://doi.org:10.1016/j.matchemphys.2006.12.008.
[50] N. Guerrini, et al., *Chem. Mater.* **2020**, *32*, 3733–3740, https://doi.org:10.1021/acs.chemmater.9b04459.
[51] J. A. Xu, et al., *ACS Appl. Energy Mater.* **2023**, *6*, 5026–5036, https://doi.org:10.1021/acsaem.3c00630.
[52] L. L. Driscoll, et al., *Energy Environ. Sci.* **2023**, https://doi.org:10.1039/d3ee00249 g.
[53] M. Freire, et al., *Nat. Mater* **2016**, *15*, 173-+, https://doi.org:10.1038/Nmat4479.
[54] J. L. Zhang, W. H. Wang, Y. S. Li, D. Y. W. Yu, *Electrochim. Acta* **2015**, *185*, 76–82, https://doi.org:10.1016/j.electacta.2015.10.101.
[55] H. Liu, et al., *ACS Materials Letters* **2019**, *1*, 96–102, https://doi.org:10.1021/acsmaterialslett.9b00099.
[56] M. Prades, N. Masó, H. Beltrán, E. Cordoncillo, A. R. West, *J. Mater. Chem.* **2010**, *20*, 5335–5344, https://doi.org:10.1039/c0jm00677g.
[57] J. A. Enterkin, et al., *Nat. Mater.* **2010**, *9*, 245–248, https://doi.org:10.1038/Nmat2636.
[58] M. Bianchini, F. Fauth, P. Hartmann, T. Brezesinski, J. Janek, *J. Mater. Chem. A* **2020**, *8*, 1808–1820, https://doi.org:10.1039/c9ta12073d.
[59] K. Luo, et al., *Nat. Chem.* **2016**, *8*, 684–691, https://doi.org:10.1038/nchem.2471.
[60] E. McCalla, et al., *Science* **2015**, *350*, 1516–1521, https://doi.org:10.1126/science.aac8260.
[61] Z. Chen, J. Li, X. C. Zeng, *J. Am. Chem. Soc.* **2019**, *141*, 10751–10759, https://doi.org:10.1021/jacs.9b03710.
[62] F. Ning, et al., *Nat. Commun* **2020**, *11*, https://doi.org:10.1038/s41467-020-18423-72020.
[63] I. I. Abate, et al., *Energy Environ. Sci.* **2021**, *14*, 4858–4867, https://doi.org:10.1039/d1ee01037a.
[64] Q. Jacquet, et al., *Chem. Mater.* **2018**, *30*, 7682–7690, https://doi.org:10.1021/acs.chemmater.8b02955.
[65] R. A. House, et al., *Nat. Commun* **2021**, *12*, https://doi.org:10.1038/s41467-021-23154-42021.
[66] J. Hong, et al., *Nat. Mater.* **2019**, *18*, 256–265, https://doi.org:10.1038/s41563-018-0276-1.

Manuscript received: May 9, 2024
Revised manuscript received: September 6, 2024
Accepted manuscript online: September 17, 2024

 © 2024 The Author(s). Zeitschrift für anorganische und allgemeine Chemie published by Wiley-VCH GmbH

15213749, 0, Downloaded from https://onlinelibrary.wiley.com/doi/10.1002/zaac.202400067 by UNIVERSITY OF SHEFFIELD, Wiley Online Library on [19/11/2024]. See the Terms and Conditions (https://onlinelibrary.wiley.com/terms-and-conditions) on Wiley Online Library for rules of use; OA articles are governed by the applicable Creative Commons License

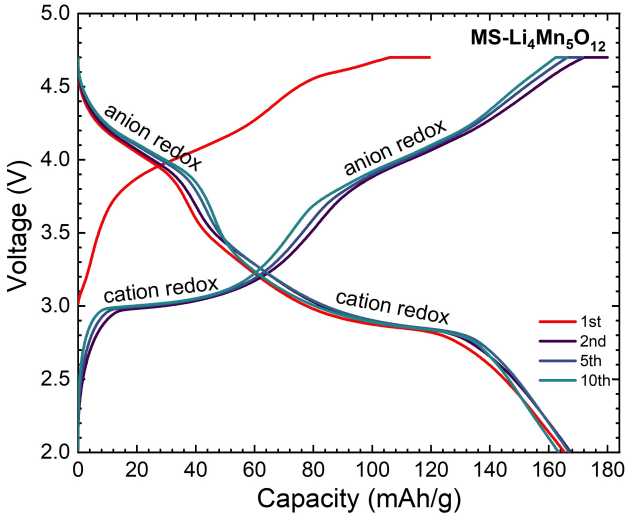

Y. Zhao, L. Middlemiss, X. Zhi, P. Gross, A. R West

15213749, 0, Downloaded from https://onlinelibrary.wiley.com/doi/10.1002/zaac.202400067 by UNIVERSITY OF SHEFFIELD, Wiley Online Library on [19/11/2024]. See the Terms and Conditions (https://onlinelibrary.wiley.com/terms-and-conditions) on Wiley Online Library for rules of use; OA articles are governed by the applicable Creative Commons License